Effective Work Function Modulation of Graphene/Carbon Nanotube Composite Films As Transparent Cathodes for Organic Optoelectronics

Jen-Hsien Huang,[†] Jheng-Hao Fang,[†] Chung-Chun Liu,[†] and Chih-Wei Chu[†,‡,*]

[†]Research Center for Applied Sciences, Academia Sinica, Taipei, Taiwan 11529 and [‡]Department of Photonics, National Chiao-Tung University, Hsinchu, Taiwan 30010

ABSTRACT In this study, we found that the work functions (Φ_w) of solution-processable, functional graphene/carbon nanotube-based transparent conductors were readily manipulated, varying between 5.1 and 3.4 eV, depending on the nature of the doping alkali carbonate salt. We used the graphene-based electrodes possessing lower values of Φ_w as cathodes in inverted-architecture polymer photovoltaic devices to effectively collect electrons, giving rise to an optimal power conversion efficiency of 1.27%.

KEYWORDS: graphene · transparent electrode · solar cells · surfactant · work function · cathode

Flexible optoelectronic devices have spurred immense interest because of their applications in displays, solar cells, sensors, and hand-held communication systems.[1−5] Highly conductive indium tin oxide (ITO) is frequently used as the transparent electrode in optoelectronic devices; diminishing indium resources, complicated processing procedures, and poor mechanical flexibility have, however, limited its widespread applications in flexible systems.

Graphene, a molecule comprising a single layer of carbon, has been touted for its excellent electrical conducting properties ever since its experimental isolation in 2004.[6] Graphene-based films have been investigated extensively for use as transparent electrodes because of their excellent optical and electrical properties.[7−14] At present, most large-scale graphene thin films are prepared through chemical vapor deposition (CVD), followed by transfer printing on a target substrate.[15,16] Unfortunately, the high processing temperature required for CVD restricts the growth of graphene to a limited number of substrates. The transfer procedure is also too complicated to scale up, and the resulting graphene samples are often readily contaminated and damaged. Although an electrochemical exfoliation method has been proposed[17,18] for the production of higher-quality graphene on a large scale, this approach does not provide stable, dispersed graphene solutions for solution processing. An alternative method for preparing large-area graphene thin films is through solution processing of suspensions of stable graphene oxide (GO).[19,20] Although the conjugated networks can be restored upon reduction in hydrazine vapor or through thermal annealing after deposition, their conductivities do not rival those of systems prepared through CVD, by virtue of the large resistance originating from the stack of individual GO pieces. In this regard, a strategy of using carbon nanotubes (CNTs) to tailor the electronic properties of GO has been proposed.[21]

In addition to requiring excellent conductivity and transparency of their electrodes, the performance of organic optoelectronic devices also relies on efficient carrier injection between the active layers and the electrodes. Modulating the work function (Φ_w) of the electrode to form an ohmic contact with the active layer can enhance the degree of charge injection, thereby improving device performance.[22,23] Accordingly, work function engineering of electrodes has been investigated extensively as a means of improving optoelectronic performance. In general, transparent electrodes based on highly conductive polymers [*e.g.*, polyaniline, poly(3,4-ethylenedioxythiophene)] or graphene possess high values of Φ_w (*ca.* 5.0−5.2 eV).[24−26] Nevertheless, functional electrodes with such high values of Φ_w can be used only as hole transport/buffer anodes in organic optoelectronic

* Address correspondence to gchu@gate.sinica.edu.tw.

Received for review April 4, 2011 and accepted June 28, 2011.

Published online June 28, 2011
10.1021/nn201253w

devices; applying them in different configurations, such as inverted or tandem solar cells, requires modification of the interface through insertion of a functional interfacial layer or chemical doping to form a low-Φ_w cathode. For graphene, the variation in the work function can be achieved through chemical doping or modification of the surface with an interfacial layer to form interface dipoles.[27−31] Recently, it was demonstrated that the presence of salts, particularly alkali-based salts, in an *n*-type interfacial layer can improve the efficiency of solar cells and thin film transistors.[32,33] These results suggested the possibility of controlling the values of Φ_w of graphene-based electrodes. In the present study, we prepared highly conductive and transparent graphene-based electrodes with tunable work functions by combining single-walled carbon nanotubes (SWCNTs) with chemically reduced graphene (rGO). To produce hybrid suspensions of rGO and CNTs, we dispersed dry powders of GO and SWCNTs directly in anhydrous hydrazine. The work functions of these carbon composite films could be tuned through doping with alkali carbonates. Upon thermal annealing, the alkali carbonates decomposed into low-Φ_w alkali oxides that covered the carbon-based materials. We used X-ray photoelectron spectrometry (XPS)/UPS spectra to measure the correlation between the work function and the nature of the doped alkali carbonates. Finally, we fabricated organic solar cells having an inverted structure to demonstrate the potential use of carbon composite electrodes with tunable values of Φ_w.

RESULTS AND DISCUSSION

The signals in the Raman spectra of SWCNTs and rGO directly reflect the stacking and functionality of the graphitic frameworks. We recorded Raman spectra of films cast from each constituent and from their hybrid. In the spectrum of the carbon composite film recorded with excitation of 514 nm, we observe (Figure 1) dominant features at 1596 and 1587 cm^{-1} (associated with the phonon transition within the 1-D SWCNTs) and at 1350 cm^{-1} (the D peak of the rGO). These signals suggest that the blended films were mixed well without severe aggregation and that they maintained the unique electronic properties of their individual carbon components.

To better understand the structural features, Figure 2 presents representative transmission electron microscopy (TEM) images of the rGO, the SWCNTs, and their all-carbon hybrid. The image of the rGO reveals its paper-like structure, with several stacking layers of monatomic rGO sheets (Figure 2a). SWCNTs can form stable solutions in hydrazine through the creation of hydrazinium compounds, comprising negatively charged SWCNTs surrounded by $N_2H_5^+$ counterions.[21,34] Although our SWCNTs formed a stable solution in hydrazine without

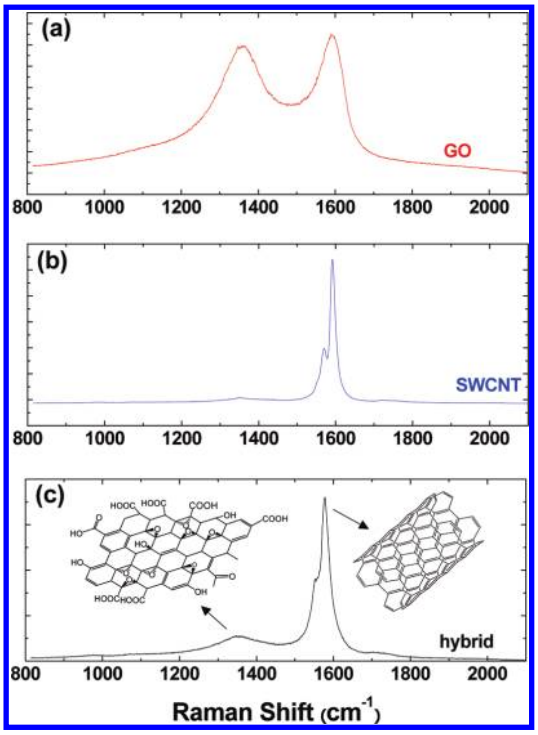

Figure 1. Raman spectroscopic characterization of chemical compositions. Representative Raman spectra of films of (a) rGO, (b) SWCNTs, and (c) the rGO-SWCNT composite. The spectrum of the carbon composite exhibits the characteristic peak originating from the SWCNTs, indicating that the electronic structure of the SWCNTs was preserved in the hybrid dispersion.

precipitation, the TEM image in Figure 2b reveals severe aggregation and many SWCNT bundles. These SWCNT aggregates and bundles underwent dispersion after sonicating with rGO for several hours (Figure 2c and d). This rGO-SWCNT colloidal dispersion was stable for several months without visible precipitation, suggesting that the rGO acted as a molecular surfactant to disperse the SWCNTs[35,36] because its paper-like structure possessed a large surface area for interaction with the SWCNTs. The abundance of highly conjugated structures on the surface of the rGO allowed it to adhere readily onto the cylindrical planes of the SWCNTs through $\pi-\pi$ interactions. Figure 2e displays a central region of the surface of the rGO-SWCNT hybrid; it reveals many SWCNTs running across the rGO surface to form a conductive network. We believe that this surfactant-free method of dispersing SWCNTs might spur research into their potential uses in optoelectronic and electronic applications.

We also used atomic force microscopy (AFM) and scanning electron microscopy (SEM) to characterize the morphologies of the single-component and composite carbon-based thin films (Figure 3). The AFM and SEM images indicate that the rGO thin film consisted of one to three layers of rGO sheets stacked on the substrate with a broad size distribution of 1−7 μm

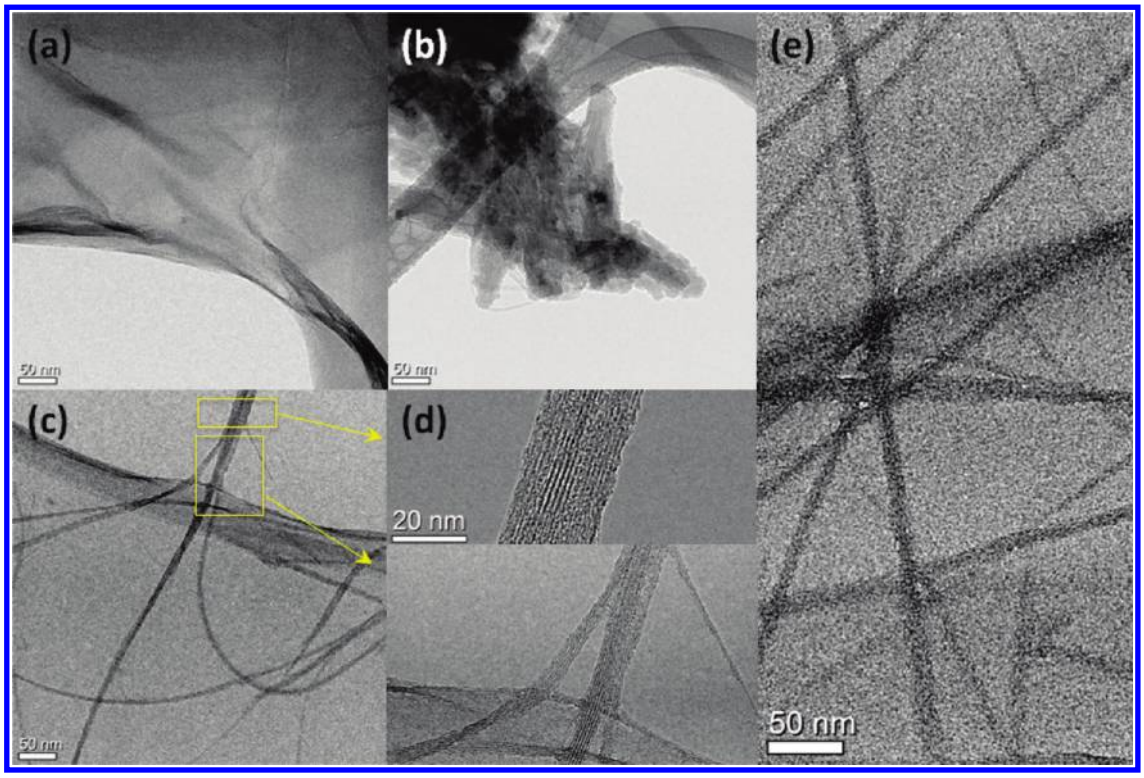

Figure 2. TEM images of dispersed solutions of rGO, SWCNTs, and rGO-SWCNTs. TEM images of (a) rGO, (b) SWCNTs, and (c–e) rGO-SWCNT composites. The low-magnification (scale bar: 50 nm) TEM images of the rGO-SWCNT composites in (c) and (d) indicate that rGO acted as a surfactant to disperse the SWCNTs through $\pi-\pi$ interactions. The high-resolution (scale bar: 20 nm) TEM image of the rGO-SWCNT composite in (d) indicates that the SWCNTs underwent debundling to become physically attached to the rGO sheets. (e) Central region of the surface of the rGO-SWCNTs, revealing many SWCNTs extended across the rGO surface.

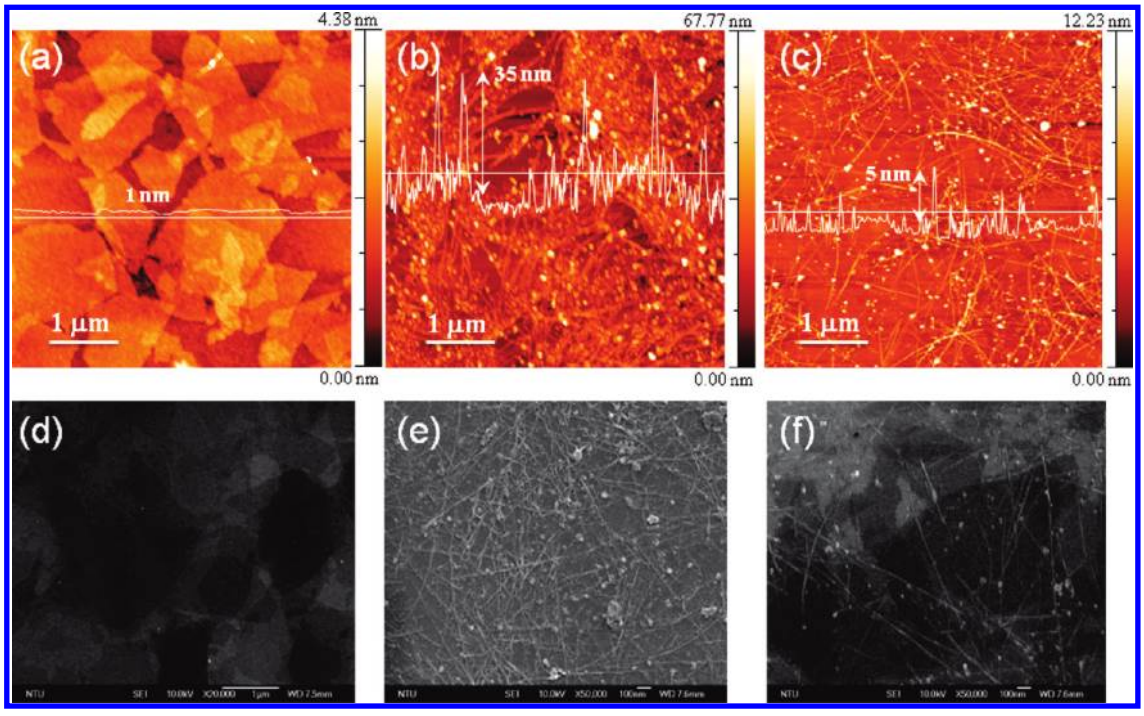

Figure 3. Representative images of the surface morphologies of the carbon-based films. (a–c) AFM images with height profiles of films of (a) rGO, (b) SWCNTs, and (c) the rGO-SWCNT composite. (d–f) Corresponding SEM images. The AFM images reveal that rGO effectively debundled the SWCNTs. The average surface roughness of the SWCNTs decreased from ca. 35 nm to ca. 5 nm after interacting with the rGO.

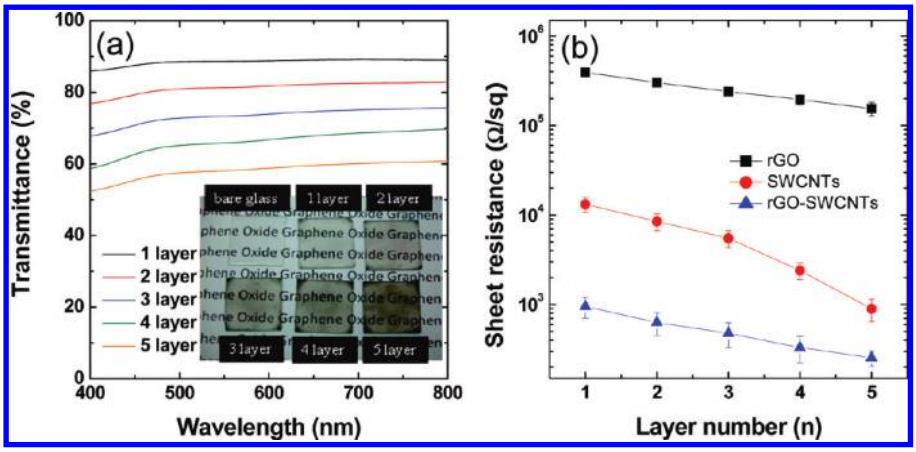

Figure 4. Transmittances and resistances of the carbon composite films. (a) Transmission spectra of rGO-SWCNT films featuring different numbers of deposited layers. Inset: photograph of the corresponding samples. (b) Sheet resistances of rGO, SWCNTs, and the hybrid combination as a function of the number of layers. The sheet resistance of rGO decreased significantly after adhering to the SWCNTs, forming an extended conjugated network with individual SWCNTs connecting the gaps between the rGO sheets. The sheet resistance was measured using a four-point probe.

(Figure 3a and d). The AFM profile revealed that the film was approximately 1−3 nm thick, consistent with one to three layers of the rGO. For the pristine SWCNTs films, the surface morphology was uneven, featuring coarse SWCNT bundles, with a roughness of approximately 7.34 nm (Figure 3b and e). In a transparent electrode, such bundles would be problematic for device fabrication because they might protrude through the active layers and, thereby, result in shorting. Consistent with the TEM images, the SWCNTs appeared to adhere to the rGO sheets through $\pi-\pi$ interactions originating from their graphitic structure. In addition, the rGO acted as a blanket, covering the SWCNTs to smooth out the surface. In the hybrid, the SWCNTs acted as a conductive bridge to connect the rGO sheets, thereby minimizing the barrier for charge transfer between the rGO sheets and decreasing the sheet resistance.

Both a smooth surface and high transparency are necessary if rGO-SWCNT films are to become effective substitutes for transparent metal oxide electrodes. We characterized the optical and electrical properties of our films using UV−vis spectroscopy (at normal incidence) and a four-point probe. The number of spin-cast layers had the most direct effect on transmittance, as revealed in the spectra and photographs presented in Figure 4. Images depicting the film thicknesses are provided in the Supporting Information. As expected, increasing the number of spin-cast layers from one to five provided thicker carbon composite films, thereby decreasing the optical transmittance at 550 nm from 88.8% to 58.7%. The inset in Figure 4b displays the corresponding sheet resistances of the rGO-SWCNT films. A lower number of spin-cast layers resulted in less material and, hence, fewer conduction pathways, leading to higher sheet resistances. For the film formed from five layers, the sheet resistance reached as low as 254 Ω sq^{-1}. Control experiments revealed that the sheet resistances of the single-component SWCNTs and rGO films cast from hydrazine were much higher than those of the rGO-SWCNT composites. We suspect that the sheet resistance would decrease further if we were to optimize the content ratio between the rGO and SWCNTs.

TABLE 1. Photovoltaic Characteristics of Inverted P3HT/PCBM Solar Cells Incorporating rGO-SWCNTs As Transparent Electrodes; Transmittance (T) at 550 nm and Sheet Resistance (R_{sh}) Data for the rGO-SWCNTs

sample	$T_{550\ nm}$ (%)	R_{sh} (Ω sq^{-1})	J_{SC} (mA cm^{-2})	V_{OC} (V)	FF (%)	PCE (%)
1 layer	88.6	954	2.76	0.55	34.2	0.51
2 layer	81.3	631	3.63	0.60	36.7	0.80
3 layer	73.3	478	4.37	0.60	39.3	1.03
4 layer	65.8	331	4.77	0.60	44.4	1.27
5 layer	58.1	254	3.89	0.58	46.4	1.18

Gratified by the performance of the rGO-SWCNT films during electrical characterization, we incorporated these materials as transparent electrodes for the fabrication of P3HT/PCBM photovoltaic (PV) devices. Table 1 summarizes the effect of the thickness of the rGO-SWCNT layer on the performance of the organic PVs; the Supporting Information presents the corresponding current−voltage characteristics. The fill factor (FF) underwent a monotonic increase from 34.2% to 46.4% upon increasing the number of layers, due to the decrease in the sheet resistance. The short-circuit current density (J_{SC}) gradually increased from 2.76 mA cm^{-2} for the single-layer rGO-SWCNT device to 4.77 mA cm^{-2} for the four-layer rGO-SWCNT device, decreasing thereafter to 3.89 mA cm^{-2} (five-layer) because of insufficient transparency. Therefore, an optimal rGO-SWCNT thickness exists for optimal PV performance. The power conversion efficiency (PCE) of the P3HT:PCBM PV device incorporating the four-layer rGO-SWCNT film was 1.27%.

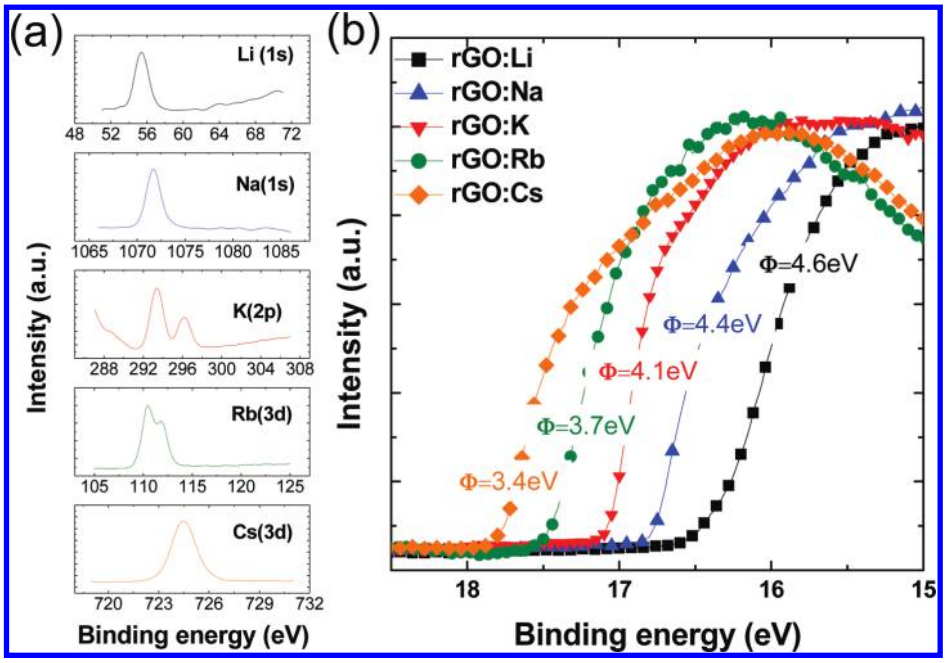

Figure 5. Measurements of the values of Φ_w of the rGO-SWCNT films after doping with various alkali carbonates. (a) XPS and (b) UPS spectra of the rGO doped with various alkali carbonates. The pronounced peaks for the alkali metals indicate the successful doping of the alkali carbonates. The work functions of the rGO-SWCNT films after doping with Li_2CO_3 and Cs_2CO_3 were 4.6 and 3.4 eV, respectively. The values of Φ_w of the rGO-SWCNT films were determined from the UPS secondary electron cutoff.

To tune the work functions of the rGO-SWCNT films and thereby develop versatile electrodes for optoelectronics, we used alkali carbonates to dope the carbon composites and modify their surfaces. We dissolved the rGO-SWCNTs and alkali carbonates in hydrazine and deionized water, respectively, and then blended them together at a 1:0.25 ratio (w/w) to form a 0.2 wt % solution. Figure 5a displays XPS spectra revealing the chemical compositions of the doped carbon composite films; these spectra featured pronounced alkali metal peaks, indicating successful doping. Figure 5b presents the absolute values of Φ_w, determined by measuring the shift in the secondary electron cutoff, of the rGO-SWCNT films incorporating different doping alkali carbonates. We observe a clear trend: the values of Φ_w of the rGO-SWCNT electrodes decreased from 4.6 eV when doped with Li_2CO_3 to 3.4 eV when doped with Cs_2CO_3. These results are consistent with those reported previously by the Yang group.[37] The doped alkali carbonates formed interfacial layers on the rGO-SWCNTs, inducing interfacial dipoles and, thereby, decreasing the work function of the carbon composites.[31,37,38] The pristine rGO-SWCNT electrode exhibited a value of Φ_w of 5.1 eV (Supporting Information); therefore, the large changes in Φ_w appear to result directly from the surface modification of the rGO-SWCNTs.

Figure 6 presents an SEM image and corresponding EDS map for the Cs_2CO_3-doped rGO-SWCNT electrode (Cs:rGO-SWCNTs). The Cs atoms were distributed homogeneously throughout the sample, suggesting that the surface of the rGO-SWCNTs had been modified with the alkali carbonate. AFM imaging of the surface morphologies of the Cs_2CO_3-doped and undoped rGO-SWCNTs revealed that the rGO sheets and SWCNTs were slightly rougher and coarser in the formed sample, suggesting that the surface of the carbon composite was decorated with Cs_2CO_3. The root-mean-square roughnesses of the doped and undoped films were 3.23 and 4.01 nm, respectively, suggesting that the doping Cs_2CO_3 layer on the surface of the carbon composite was only a few monolayers thick (*i.e.*, the surface roughness was almost unchanged). To study the effect of alkali carbonate on electrode conductivity, we also measured the sheet resistances of the various electrodes (Supporting Information), finding that the graphene-based electrodes maintained their conductivity in the presence of a trace amount of dopant (0.05 wt %).

To demonstrate the effect of the shift in the values of Φ_w on the PV performance, we used the doped rGO-SWCNT films to fabricate P3HT:PCBM PVs possessing an inverted architecture. We thermally annealed all of the doped rGO-SWCNT films at 200 °C for 30 min prior to deposition of the active layer. Figure 7a reveals that the presence of a thin layer of each of the alkali carbonates decreased the value of Φ_w of the rGO-SWCNTs, but to different extents. Upon varying the dopant of the rGO-SWCNTs from Li_2CO_3 to Cs_2CO_3, the open-circuit voltage (V_{OC}) and FF of the corresponding devices increased from 0.26 V/25.4% to 0.57 V/42.9%, respectively, consistent with the shift in the work

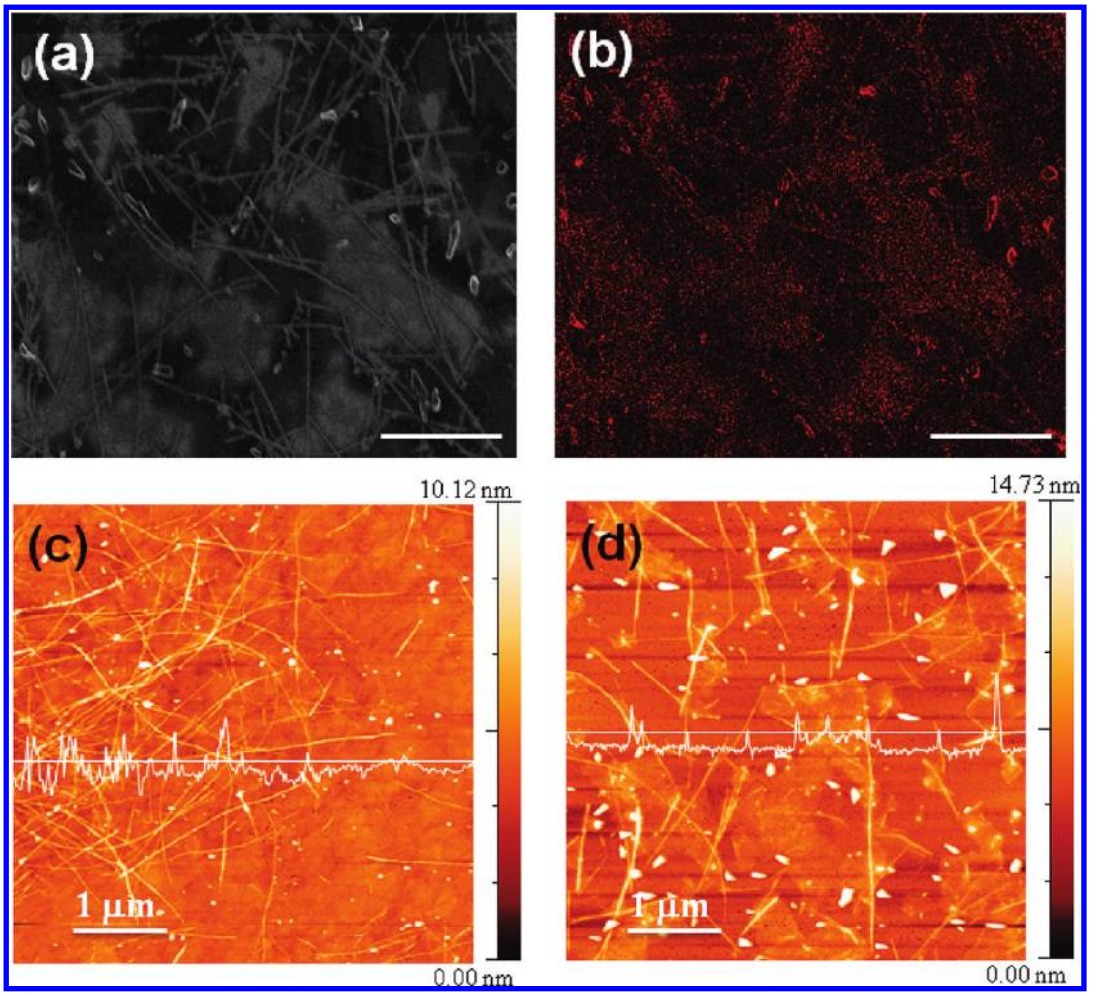

Figure 6. Elemental distribution and surface morphology of the rGO-SWCNT film after doping with Cs_2CO_3. (a) SEM image and (b) corresponding EDS map for the Cs:rGO-SWCNT film (scale bar: 1 μm). The red dots represent signals from Cs elements. The EDS elementary map reveals that the Cs atoms were distributed homogeneously throughout the basal plane of the rGO sheet and the circumferential plane of the SWCNTs. AFM images of films of (c) rGO-SWCNTs and (d) Cs:rGO-SWCNTs, revealing that the SWCNTs were slightly thicker after doping and that the surface of the rGO film was covered with a thin layer of Cs_2CO_3.

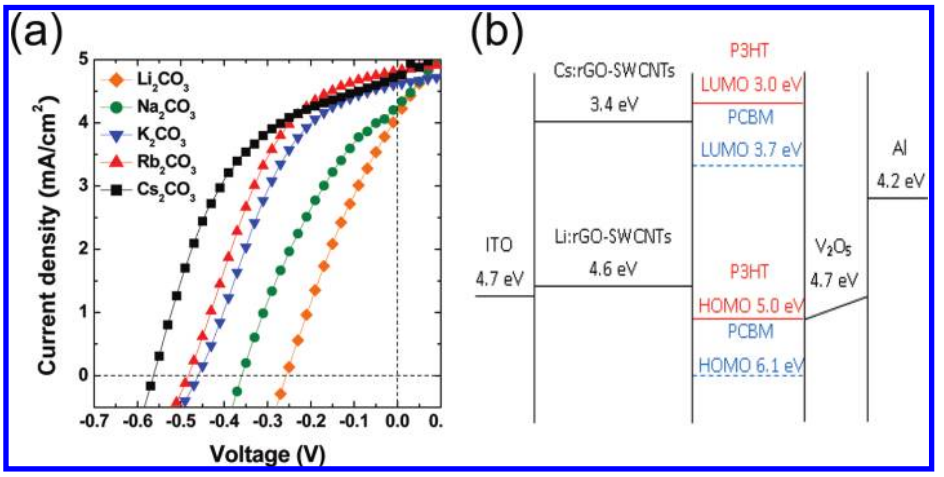

Figure 7. Effect of dopant on inverted cell performance. (a) *J*–*V* characteristics of the inverted P3HT/PCBM solar cells incorporating rGO-SWCNT doped with various alkali carbonates as the cathode. (b) Energy level diagrams of inverted solar cells featuring alkali carbonate-doped carbon-based cathodes.

function. The device incorporating the Cs_2CO_3-doped electrode exhibited a PCE of 1.13%, indicating that enhanced charge injection occurred as a result of the shift in the value of Φ_w.[35] Figure 7b displays the energy

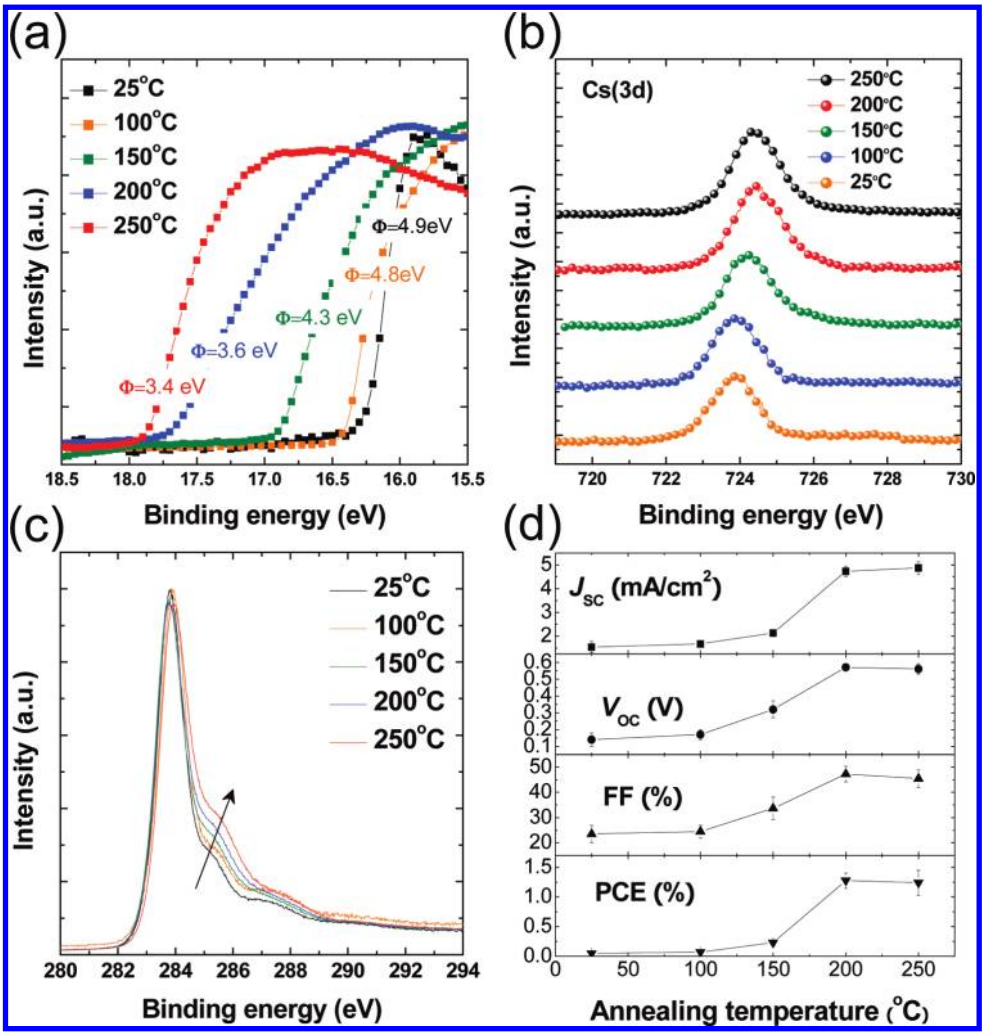

Figure 8. Determining the mechanism for the variation in work function of rGO-SWCNT films after doping with Cs_2CO_3. (a) UPS spectra and (b) XPS spectra (Cs 3d) of Cs:rGO-SWCNT films that had been subjected to annealing at various temperatures. The signature peak of the Cs 3d energy level shifted to higher binding energy after thermal annealing, a conclusive indication that Cs_2CO_3 decomposed into cesium oxide. (c) XPS spectra of rGO-SWCNT films presenting a thin layer of Cs_2CO_3 that had been subjected to annealing at various temperatures. After thermal annealing, the increased intensity of the shoulder located at higher binding energy indicates the formation of C−O−Cs complexes. (d) Performances of P3HT/PCBM inverted cells incorporating Cs:rGO-SWCNT films that had been subjected to annealing at various temperatures.

levels of the individual layers and illustrates the mechanism of the solar cells. The value of Φ_w of the Li:rGO-SWCNT device (4.6 eV) decreased to 3.4 eV for the Cs:rGO-SWCNT device. The work function tuning improved the match between the values of Φ_w of the transparent electrode and the lowest unoccupied molecular orbital (LUMO) of PCBM (3.7 eV), leading to a stronger built-in field and increased charge collection.[39]

To better understand the mechanism responsible for the variation of the work function after doping with alkali carbonates, we also used UPS to evaluate the values of Φ_w of Cs:rGO-SWCNT devices that we had prepared using different annealing temperatures (Figure 8a). Without thermal annealing, the value of Φ_w of the Cs:rGO-SWCNT device was 4.9 eV, close to that of the pristine rGO-SWCNTs (5.1 eV). The work function of the Cs:rGO-SWCNT device decreased from 4.9 to 3.4 eV upon increasing the annealing temperature to 250 °C. To gain more insight into the chemical reaction between Cs_2CO_3 and rGO-SWCNT, we used XPS to monitor the chemical shift of the Cs 3d signals. Figure 8b reveals that the Cs 3d signal shifted to higher binding energy upon annealing, consistent with decomposition to form stoichiometric Cs_2O doped with Cs_2O_2 and CsO_2.[40,38] The thermal decomposition of Cs salts leads to the formation of cesium oxide with higher ion valence level,[41] resulting in cesium oxide behaving as an electron-transporting layer having a relatively low work function; therefore, the electron injection properties improved after annealing treatment. Moreover, we also recorded the C 1s signals to study the properties of the interface between rGO-SWCNT and Cs_2CO_3. For this measurement, we spin-cast a very thin layer of Cs_2CO_3 onto rGO-SWCNT films and then subjected them to different annealing temperatures. This approach allowed us to monitor the reaction occurring at the interface

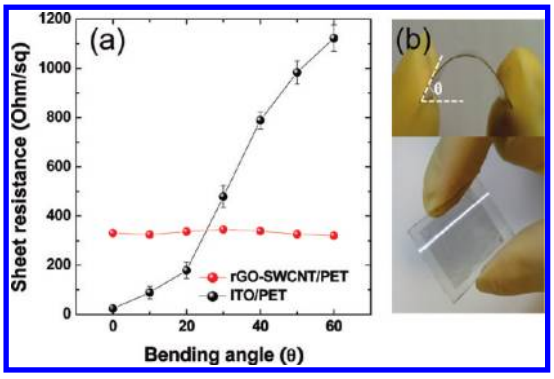

Figure 9. Bending tests of films of ITO and rGO-SWCNTs on flexible PET substrates. (a) Sheet resistances of rGO-SWCNT and ITO films on PET substrates, plotted with respect to the bending angle. (b) Representative photographs of an rGO-SWCNT flexible electrode subjected to bending.

between the contact layer of rGO-SWCNT and Cs_2CO_3. Figure 8c presents spectra displaying the C 1s signal. After thermal annealing of the thin films, a shoulder appeared at high binding energy, indicating the formation of strong chemical bonds between the carbon materials and Cs_2CO_3 layer.[42] We suspect that the interfacial monolayer of C−O−Cs complexes that forms during treatment at high temperature[42] acted as an additional dipole to further reduce the value of Φ_w. This interfacial complex has an even lower work function than that of decomposed Cs_2CO_3.[42] The presence of similar complexes, including W−O−Cs,[43] Si−O−Cs,[44] Ga−O−Cs,[45] and Al−O−Cs,[38] can also produce low-Φ_w surfaces. Figure 8d presents the performance parameters of the inverted cells incorporating Cs:rGO-SWCNT electrodes that had been annealed at various temperatures. For the Cs:rGO-SWCNTs that had not experienced thermal annealing, the PCE was 0.05%. The performance of each device improved when the Cs:rGO-SWCNT layer had been subjected to annealing. When the annealing temperature of the Cs:rGO-SWCNT layer increased from room temperature to 200 °C, the PCE increased from 0.05% to 1.27%. In addition, all of the other device characteristics—J_{SC}, V_{OC}, and FF—improved as well. The significant improvements in the inverted devices' performance resulted from the lowering of the work function of the Cs:rGO-SWCNT electrodes.

To investigate the flexibility of the rGO-SWCNT electrodes, we used the sheet resistance as a parameter for exploring the stability of the rGO-SWCNT and ITO films under various bending conditions. Figure 9 displays the correlation between bending angle and conductance for the rGO-SWCNT and ITO films. The ITO film underwent an irreversible loss of electrical conductivity, due to the propagation of cracks throughout its crystalline network; the sheet resistance increased from 24 to 1123 Ω sq^{-1} after blending at 60°. Meanwhile, the rGO-SWCNT film exhibited comparable sheet resistances before and after performing the bending test cycle (247 and 244 Ω sq^{-1}, respectively), by virtue of its high flexibility and mechanical strength (see the Supporting Information). These measurements suggest that the carbon-based hybrid composite film possessed much greater mechanical flexibility than that of the ITO film, making it well-suited for use as a conductive platform for flexible electronics.

CONCLUSIONS

We have developed a high-throughput, facile strategy for tuning the value of Φ_w of solution-processed rGO-SWCNT films through systematic doping with alkali carbonates, potentially opening up a new route toward Φ_w-tunable graphitic materials. The alkaline-doped carbon-based hybrid electrodes are readily employed as functional electrodes in inverted PVs exhibiting much-improved efficiencies. The ability to tailor the electrical properties of graphene-based transparent electrodes should boost the development of flexible and ITO-free optoelectronics.

EXPERIMENTAL SECTION

Materials. All chemicals were purchased from Sigma−Aldrich and used as received. GO was prepared from graphite powder (Bay Carbon, SP-1) using a modified version of Hummers' method.[46] Briefly, graphite (2 g), $NaNO_3$ (1 g), and H_2SO_4 (46 mL) were stirred together in an ice bath, and then $KMnO_4$ (6 g) was added slowly. Once mixed, the solution was transferred to a water bath and stirred at 35 °C for ca. 1 h, forming a thick paste. Water (80 mL) was added, and then the solution was stirred for 1 h at 90 °C. Finally, more water (200 mL) was added, followed by the slow addition of H_2O_2 (30%, 6 mL). The warm solution was filtered and washed sequentially with 10% HCl (3 × 200 mL) and water (200 mL). The filter cake was dispersed in water through mechanical agitation and stirred overnight. The dispersion was left to settle; the supernatant (clear yellow dispersion) was subjected to dialysis for 1 month, resulting in a stock solution having a GO concentration of ca. 0.17 mg mL^{-1}. The stable dispersion was filtered through an alumina membrane and left to dry for several days. The GO paper was then carefully peeled from the filter and stored under ambient conditions. To produce hybrid suspensions of rGO and SWCNTs, dry powders of GO and SWCNTs were dispersed directly in anhydrous hydrazine and left to stir for 1 week. Hydrazine bubbled violently upon contact with the GO and SWCNT powders, but soon formed a uniform dark gray suspension with no visible precipitation. XPS spectra of the GO and rGO (dispersed in hydrazine) are provided in the Supporting Information. Once the stirring was complete, the stable dispersion was centrifuged to separate out any SWCNT bundles and aggregated rGO. After centrifugation, the uniformity of a given rGO-SWCNT dispersion was ensured through heating to 60 °C with repeated ultrasonic agitation (VWR model 250D sonicator; set at level 9) for 30 min.

Solar Cell Devices. The polymer solar cells consisted of a layer of the P3HT/PCBM blend thin film sandwiched between the rGO-SWCNT electrode and a metal cathode. Precleaned glass substrates were treated with O_2 plasma to activate the surface. Typically, a mixture of GO (1 mg mL^{-1}) and SWCNTs (5 mg mL^{-1})

in hydrazine was used for spin-coating on the hydrophilic glass substrates. The device structure included a thin PEDOT:PSS buffer layer, upon which was spin-coated and "slow-grown" a layer of P3HT/PCBM (1:1, w/w; 2% in dichlorobenzene).[47] Finally, thermal evaporation of Al and Ca provided the reflective cathodes. For the inverted cell, rGO-SWCNT films incorporating alkali carbonates were spin-cast onto the precleaned glass substrates. The P3HT/PCBM layer was then cast from dichlorobenzene onto the carbon-based electrode. Finally, thermal evaporation of Al and V_2O_5 provided the reflective anodes.

Characterization. An alpha 300 Raman spectrometer (WITec Instruments, Germany) was used to analyze the chemical compositions of the carbon composite films with a fixed wavelength of 514.5 nm. The surface morphologies of the carbon composite films were investigated using AFM (Digital Instrument NS 3a controller equipped with a D3100 stage) and SEM (Hitachi S-4700). The transmittance spectra of the carbon composite films were obtained using a Jasco-V-670 UV−vis spectrophotometer. The conductivities of the transparent electrodes were analyzed using a four-point probe. XPS/UPS spectra were recorded using a PHI 5000 VersaProbe (ULVAC-PHI, Chigasaki, Japan) system with He(I) ($h\nu$ = 21.2 eV) as the energy source. Solar cell testing was performed inside a glovebox under simulated AM 1.5G irradiation (100 W cm^{-2}) using a Xe lamp-based solar simulator (Thermal Oriel 1000 W). The light source was a 450 W Xe lamp (Oriel Instrument, model 6266) equipped with a water-based IR filter (Oriel Instrument, model 6123NS). The light output from the monochromator (Oriel Instrument, model 74100) was focused onto the tested PV cell. Electrical characteristics were measured at room temperature under a N_2 environment using an HP 4156C apparatus placed within a glovebox.

Acknowledgment. We thank the National Science Council (NSC) of Taiwan (NSC 99-2221-E-001-012) and the Academia Sinica Research Program on Nanoscience and Nanotechnology for financial support. We thank Dr. Vincent Tung and Prof. Jiaxing Huang at Northwestern for technical assistance and helpful discussions.

Supporting Information Available: *J*−*V* characteristics of P3HT/PCBM solar cells incorporating rGO-SWCNT films as transparent electrodes; UPS spectrum of an rGO-SWCNT film spin-coated on a Si substrate; optical images of the ITO/PET film before and after bending; XPS spectra of the GO and rGO reduced through treatment with hydrazine; images of the thicknesses of carbon-based films possessing different numbers of cast layers; sheet resistances of graphene-based electrodes incorporating different dopants. This material is available free of charge *via* the Internet at http://pubs.acs.org.

REFERENCES AND NOTES

1. Wang, L.; Swensen, J. S.; Polikarpov, E.; Matson, D. W.; Bonham, C. C.; Bennett, W.; Gaspar, D. J.; Padmaperuma, A. B. Highly Efficient Blue Organic Light-Emitting Devices with Indium-Free Transparent Anode on Flexible Substrates. *Org. Electron.* **2010**, *11*, 1555–1560.
2. Qi, Y.; McAlpine, M. C. Nanotechnology-Enabled Flexible and Biocompatible Energy Harvesting. *Energy Environ. Sci.* **2010**, *3*, 1275–1285.
3. Krebs, F. C.; Nielsen, T. D.; Fyenbo, J.; Wadstrømc, M.; Pedersen, M. S. Manufacture, Integration and Demonstration of Polymer Solar Cells in a Lamp for the "Lighting Africa" Initiative. *Energy Environ. Sci.* **2010**, *3*, 512–525.
4. Lian, K.; Li, R.; Wanga, H.; Lu, Z.; Zhang, J. DC and AC Analyses of a Printed Flexible Memory Device. *Org. Electron.* **2010**, *11*, 1141–1144.
5. Zhang, F.; Funahashi, M.; Tamaoki, N. Flexible Field-Effect Transistors from a Liquid Crystalline Semiconductor by Solution Processes. *Org. Electron.* **2010**, *11*, 363–368.
6. Novoselov, K. S.; Geim, A. K.; Morozov, S. V.; Jiang, D.; Zhang, Y.; Dubonos, S. V.; Grigorieva, I. V.; Firsov, A. A. Electric Field Effect in Atomically Thin Carbon Films. *Science* **2004**, *306*, 666–669.
7. De Arco, L. G.; Zhang, Y.; Schlenker, C. W.; Ryu, K.; Thompson, M. E.; Zhou, C. Continuous, Highly Flexible, and Transparent Graphene Films by Chemical Vapor Deposition for Organic Photovoltaics. *ACS Nano* **2010**, *4*, 2865–2873.
8. Choe, M.; Lee, B. H.; Jo, G.; Park, J.; Park, W.; Lee, S.; Hong, W. K.; Seong, M. J.; Kahng, Y. H.; Lee, K.; *et al*. Efficient Bulk-Heterojunction Photovoltaic Cells with Transparent Multi-Layer Graphene Electrodes. *Org. Electron.* **2010**, *11*, 1864–1869.
9. Geng, J.; Liu, L.; Yang, S. B.; Youn, S. C.; Kim, D. W.; Lee, J. S.; Choi, J. K.; Jung, H. T. A Simple Approach for Preparing Transparent Conductive Graphene Films Using the Controlled Chemical Reduction of Exfoliated Graphene Oxide in an Aqueous Suspension. *J. Phys. Chem. C* **2010**, *114*, 14433–14440.
10. Kalita, G.; Matsushima, M.; Uchida, H.; Wakita, K.; Umeno, M. Graphene Constructed Carbon Thin Films as Transparent Electrodes for Solar Cell Applications. *J. Mater. Chem.* **2010**, *20*, 9713–9717.
11. Hong, T. K.; Lee, D. W.; Choi, H. J.; Shin, H. S.; Kim, B. S. Transparent, Flexible Conducting Hybrid Multilayer Thin Films of Multiwalled Carbon Nanotubes with Graphene Nanosheets. *ACS Nano* **2010**, *4*, 3861–3868.
12. Chang, H.; Wang, G.; Yang, A.; Tao, X.; Liu, X. A Transparent, Flexible, Low-Temperature, and Solution Processable Graphene Composite Electrode. *Adv. Funct. Mater.* **2010**, *20*, 2893–2902.
13. Park, H.; Rowehl, J. A.; KangKim, K.; Bulovic, V.; Kong, J. Doped Graphene Electrodes for Organic Solar Cells. *Nanotechnology* **2010**, *21*, 505204–505210.
14. Li, X.; Zhu, Y.; Cai, W.; Borysiak, M.; Han, B.; Chen, D.; Piner, R. D.; Colombo, L.; Ruoff, R. S. Transfer of Large-Area Graphene Films for High-Performance Transparent Conductive Electrodes. *Nano Lett.* **2009**, *9*, 4359–4363.
15. Kim, K. S.; Zhao, Y.; Jang, H.; Lee, S. Y.; Kim, J. M.; Kim, K. S.; Ahn, J. H.; Kim, P.; Choi, J. Y.; Hong, B. H. Large-Scale Pattern Growth of Graphene Films for Stretchable Transparent Electrodes. *Nature* **2009**, *457*, 706–710.
16. Li, X.; Cai, W.; An, J.; Kim, S.; Nah, J.; Yang, D.; Piner, R.; Velamakanni, A.; Jung, I.; Tutuc, E.; *et al*. Large-Area Synthesis of High-Quality and Uniform Graphene Films on Copper Foils. *Science* **2009**, *324*, 1312–1314.
17. Hernandez, Y.; Nicolosi, V.; Lotya, M.; Blighe, F. M.; Zhenyu, S.; De, S.; McGovern, I. T.; Holland, B.; Byrne, M.; Gun, Y.; *et al*. High-Yield Production of Graphene by Liquid-Phase Exfoliation of Graphite. *Nat. Nanotechnol.* **2008**, *3*, 563–568.
18. Su, C. Y.; Lu, A. Y.; Xu, Y.; Chen, F. R.; Khlobystov, A. N.; Li, L.-J. High-Quality Thin Graphene Films from Fast Electrochemical Exfoliation. *ACS Nano* **2011**, *5*, 2332–2341.
19. Eda, G.; Fanchini, G.; Chhowalla, M. Large-Area Ultrathin Films of Reduced Graphene Oxide as a Transparent and Flexible Electronic Material. *Nat. Nanotechnol.* **2008**, *3*, 270–274.
20. Wu, J.; Agrawal, M.; Becerril, H. A.; Bao, Z.; Liu, Z.; Chen, Y.; Peumans, P. Organic Light-Emitting Diodes on Solution-Processed Graphene Transparent Electrodes. *ACS Nano* **2010**, *4*, 43–48.
21. Tung, V. C.; Chen, L. M.; Allen, M. J.; Wassei, J. K.; Nelson, K.; Kaner, R. B.; Yang, Y. Low-Temperature Solution Processing of Graphene-Carbon Nanotube Hybrid Materials for High-Performance Transparent Conductors. *Nano Lett.* **2009**, *9*, 1949–1955.
22. Cox, P. A. *The Electronic Structure and Chemistry of Solids*; Oxford University Press: New York, 1987; p 259.
23. Shi, Y. M.; Luo, S. C.; Fang, W. J.; Zhang, K. K.; Ali, E. M.; Boey, F. Y. C.; Ying, J. Y.; Wang, J. L.; Yu, H. H.; Li, L. J. Work Function Engineering of Electrodes *via* Electropolymerization of Ethylenedioxythiophenes and its Derivatives. *Org. Electron.* **2008**, *9*, 859–863.
24. Jung, J. W.; Lee, J. U.; Jo, W. H. High-Efficiency Polymer Solar Cells with Water-Soluble and Self-Doped Conducting Polyaniline Graft Copolymer as Hole Transport Layer. *J. Phys. Chem. C* **2010**, *114*, 633–637.
25. Chang, M. Y.; Wu, C. S.; Chen, Y. F.; Hsieh, B. Z.; Huang, W. Y.; Ho, K. S.; Hsieh, T. H.; Han, Y. K. Polymer Solar Cells

Incorporating One-Dimensional Polyaniline Nanotubes. *Org. Electron.* **2008**, *9*, 1136–1139.
26. Li, S. S.; Tu, K. H.; Lin, C. C.; Chen, C. W.; Chhowalla, M. Solution-Processable Graphene Oxide as an Efficient Hole Transport Layer in Polymer Solar Cells. *ACS Nano* **2010**, *4*, 3169–3174.
27. Schedin, F.; Geim, A. K.; Morozov, S. V.; Hill, E. W.; Blake, P.; Katsnelson, M. I.; Novoselov, K. S. Detection of Individual Gas Molecules Adsorbed on Graphene. *Nat. Mater.* **2007**, *6*, 652–655.
28. Dong, X. C.; Fu, D. L.; Fang, W. J.; Shi, Y. M.; Chen, P.; Li, L. J. Doping Single-Layer Graphene with Aromatic Molecules. *Small* **2009**, *5*, 1422–1426.
29. Benayad, A.; Shin, H. J.; Park, H. K.; Yoon, S. M.; Kim, K. K.; Jin, M. H.; Jeong, H. K.; Lee, J. C.; Choi, J. Y.; Lee, Y. H. Controlling Work Function of Reduced Graphite Oxide with Au-Ion Concentration. *Chem. Phys. Lett.* **2009**, *475*, 91–95.
30. Shi, Y.; Kim, K. K.; Reina, A.; Hofmann, M.; Li, L. J.; Kong, J. Work Function Engineering of Graphene Electrode *via* Chemical Doping. *ACS Nano* **2010**, *4*, 2689–2694.
31. Jo, G.; Na, S. I.; Oh, S. H.; Lee, S.; Kim, T. S.; Wang, G.; Choe, M.; Park, W.; Yoon, J.; Kim, D. Y.; *et al*. Tuning of a Graphene-Electrode Work Function to Enhance the Efficiency of Organic Bulk Heterojunction Photovoltaic Cells with an Inverted Structure. *Appl. Phys. Lett.* **2010**, *97*, 213301–213301-3.
32. Huang, J.; Watanabe, T.; Ueno, K.; Yang, Y. Highly Efficient Red-Emission Polymer Phosphorescent Light-Emitting Diodes Based on Two Novel Tris(1-phenylisoquinolinato-*C*2,*N*)iridium(III) Derivatives. *Adv. Mater.* **2007**, *19*, 739–743.
33. Chu, C. W.; Sung, C. F.; Lee, Y. Z.; Cheng, K. Improved Performance in *n*-Channel Organic Thin Film Transistors by Nanoscale Interface Modification. *Org. Electron.* **2008**, *9*, 262–266.
34. Mitzi, D. B.; Copel, M.; Chey, S. J. Low-Voltage Transistor Employing a High-Mobility Spin-Coated Chalcogenide Semiconductor. *Adv. Mater.* **2005**, *17*, 1285–1289.
35. Cote, L. J.; Kim, F.; Huang, J. X. Langmuir–Blodgett Assembly of Graphite Oxide Single Layers. *J. Am. Chem. Soc.* **2009**, *131*, 1043–1049.
36. Kim, F.; Cote, L. J.; Huang, J. X. Graphene Oxide: Surface Activity and Two-Dimensional Assembly. *Adv. Mater.* **2010**, *22*, 1954–1958.
37. Huang, J.; Li, G.; Yang, Y. A Semi-Transparent Plastic Solar Cell Fabricated by a Lamination Process. *Adv. Funct. Mater.* **2008**, *20*, 415–419.
38. Huang, J.; Xu, Z.; Yang, Y. Low-Work-Function Surface Formed by Solution-Processed and Thermally Deposited Nanoscale Layers of Cesium Carbonate. *Adv. Funct. Mater.* **2007**, *17*, 1966–1973.
39. Yuan, Y.; Reece, T. J.; Sharma, P.; Poddar, S.; Ducharme, S.; Gruverman, A.; Yang, Y.; Huang, J. Efficiency Enhancement in Organic Solar Cells with Ferroelectric Polymers. *Nat. Mater.* **2011**, *10*, 296–302.
40. Liao, H. H.; Chen, L. M.; Xu, Z.; Li, G.; Yang, Y. Highly Efficient Inverted Polymer Solar Cell by Low Temperature Annealing of Cs_2CO_3 Interlayer. *Appl. Phys. Lett.* **2008**, *92*, 173303–173303-3.
41. Sommer, A. H. Hypothetical Mechanism of Operation of the Ag-O-Cs (*S*-1) Photocathode Involving the Peroxide Cs_2O_2. *J. Appl. Phys.* **1980**, *51*, 1254–1255.
42. Pickett, W. E. Negative Electron Affinity and Low Work Function Surface: Cesium on Oxygenated Diamond (100). *Phys. Rev. Lett.* **1994**, *73*, 1664–1667.
43. Desplat, J. L. Auger Electron Spectroscopy of Cesium Adsorbed on Clean and Oxygen Covered (100) Tungsten. *Surf. Sci.* **1973**, *13*, 689–691.
44. Martinelli, R. U. Thermionic Emission from the Si/Cs/O (100) Surface. *J. Appl. Phys.* **1974**, *45*, 1183–1190.
45. Levine, J. D.; Gelhaus, F. E. Oxygen as a Beneficial Additive in Cesium Thermionic Energy Converters. *J. Appl. Phys.* **1967**, *38*, 892–893.
46. Hummers, W. S.; Offeman, R. E. Preparation of Graphitic Oxide. *J. Am. Chem. Soc.* **1958**, *80*, 1339–1339.
47. Li, G.; Shrotriya, V.; Huang, J.; Yao, Y.; Moriarty, T.; Emery, K.; Yang, Y. High-Efficiency Solution Processable Polymer Photovoltaic Cells by Self-Organization of Polymer Blends. *Nat. Mater.* **2005**, *4*, 864–868.